Article

Optimization of the Synthesis and Energy Transfer of Ca$_2$MgWO$_6$:Cr^{3+},Nd^{3+}

Viktor Anselm *[iD] and Thomas Jüstel [iD]

Department of Chemical Engineering, FH Münster University of Applied Sciences, Stegerwaldstrasse 39, D-48565 Steinfurt, Germany; tj@fh-muenster.de
* Correspondence: viktor.anselm@fh-muenster.de

Abstract: This work pertains to Cr^{3+} and Nd^{3+} co-activated Ca$_2$MgWO$_6$ phosphors synthesized by high temperature solid-state method using oxides and carbonates as raw materials. All luminescent samples according to Ca$_2$MgWO$_6$:Cr^{3+},Nd^{3+} include Cr^{3+} for the absorption of UV and visible radiation (230–800 nm) prior to energy transfer to Nd^{3+}. As a result of the energy transfer between Cr^{3+} and Nd^{3+}, we observe line emission originating from Nd^{3+} in the near infrared range additionally to the broad band near infrared emission from Cr^{3+} assigned to the spin-allowed $^4T_2 \rightarrow {^4A_2}$ transition. The energy transfer from Cr^{3+} to Nd^{3+} is discussed via the variations of the lifetime data of Cr^{3+} and Nd^{3+}. The strong absorption of Cr^{3+} in the ultraviolet range and the efficient energy transfer from Cr^{3+} to Nd^{3+} indicate that the herein presented material type can serve as a radiation converter for near infrared region light emitting diodes (NIR-LEDs) comprising an UV-A emitting (Al,Ga)N chip.

Keywords: energy transfer; Tungstates; luminescent materials; NIR emission; time-dependent spectroscopy

1. Introduction

Cr^{3+} is a widely applied activator ion in phosphors or solid state lasers emitting in the near infrared region (NIR) [1]. NIR radiation sources have a broad area of application in biomedical imaging, phototherapy, thermography, optical communication, and environment monitoring [2–6].

Incandescent and halogen lamps, silicon carbide heating elements, as well as GaAs or (Al,Ga)As LEDs are commonly used as NIR emitters. However, the application of these NIR sources is hampered by low efficiency, size, and (for NIR LEDs) their poor thermal stability, low electroluminescence efficiency, and sensitivity towards humidity [7]. To solve these problems, we can use LEDs based on a blue or UV-A emitting (Al,Ga)N semiconductor chip in combination with a suitable NIR emitting phosphor.

The rare earth ion Nd^{3+} offers suitable energy levels which, subsequent to an excitation process, lead to emission in the near infrared range and is therefore particularly well suited for application as a luminescent converter [8]. However, Nd^{3+} doped phosphors always exhibit narrow-band absorption features in the blue to ultraviolet region with a rather low absorption cross section due to the involved parity forbidden 4f–4f transitions. To overcome this drawback, the use of Cr^{3+} as a broadband sensitizer is widely discussed, since it exhibits up to three broad absorption bands in the near ultraviolet and visible spectral range due to its spin-allowed $^4A_2/^4T_2$ and $^4A_2/^4T_1$ transitions [9].

Ca$_2$MgWO$_6$ (CMW) is a low-cost material with high chemical and physical stability, which can be synthesized by a rather simple synthesis pathway and which can be doped with transition metal ions as soon as with rare earth metal ions [10]. In the past, several phosphors with CMW host have been reported, such as CMW:Eu^{3+} [11], CMW:Bi^{3+} [12], CMW:Bi^{3+},Sm^{3+} [13], CMW:Bi^{3+},Eu^{3+} [14], CMW:Er^{3+},Yb^{3+} [15], and CMW:Mn^{4+} [16]. Xu et al. studied CMW:Cr^{3+} and CMW:Cr^{3+},Yb^{3+}. It turned out that Cr^{3+} in this host material can be very efficiently excited in the ultraviolet range [17,18].

Therefore, this work deals with the synthesis of this material by solid state reaction and the investigation of the energy transfer from Cr^{3+} to Nd^{3+} in a set of CMW:Cr^{3+},Nd^{3+} samples. After having confirmed the presence of single-phase materials, diffuse reflectance spectra and luminescence properties such as excitation spectra, emission spectra, and time-dependent spectroscopy were recorded.

2. Experimental Section

For the synthesis of the compounds according to Table 1, we used the high temperature solid state synthesis. Stoichiometric amounts of the educts $CaCO_3$, MgO, WO_3, Na_2CO_3, Li_2CO_3, Cr_2O_3, and Nd_2O_3 were used, and these were ground in agate mortar with the addition of acetone. The mixture was then dried and transferred to a corundum crucible. The samples were first heated for 2 h at 600 °C and then for 5 h at 1300 °C. Between the heating steps and after the final sintering, the sinter bodies were ground again to obtain a fine beige powder.

Table 1. Stoichiometric details of prepared samples.

Sample Number	Atom-% Cr^{3+}	Atom-% Nd^{3+}	Atom-% Li^+	Atom-% Na^+	Formula
1	0	0	0	0	Ca_2MgWO_6
2	1	0	2	0	$Ca_2Mg_{0.97}Cr_{0.01}Li_{0.02}WO_6$
3	1	0.5	2	1	$Ca_{1.97}Nd_{0.01}Na_{0.02}Mg_{0.97}Cr_{0.01}Li_{0.02}WO_6$
4	1	1	2	2	$Ca_{1.94}Nd_{0.02}Na_{0.04}Mg_{0.97}Cr_{0.01}Li_{0.02}WO_6$
5	1	1.5	2	3	$Ca_{1.91}Nd_{0.03}Na_{0.06}Mg_{0.97}Cr_{0.01}Li_{0.02}WO_6$
6	1	2	2	4	$Ca_{1.88}Nd_{0.04}Na_{0.08}Mg_{0.97}Cr_{0.01}Li_{0.02}WO_6$
7	1	4	2	8	$Ca_{1.76}Nd_{0.08}Na_{0.16}Mg_{0.97}Cr_{0.01}Li_{0.02}WO_6$
8	1	6	2	12	$Ca_{1.64}Nd_{0.16}Na_{0.24}Mg_{0.97}Cr_{0.01}Li_{0.02}WO_6$
9	1	8	2	16	$Ca_{1.52}Nd_{0.16}Na_{0.32}Mg_{0.97}Cr_{0.01}Li_{0.02}WO_6$
10	1	0	0	0	$Ca_2Mg_{0.99}Cr_{0.01}WO_6$
11	1	0	1	0	$Ca_2Mg_{0.98}Cr_{0.01}Li_{0.01}WO_6$
12	0	1	0	0	$Ca_{1.98}Nd_{0.02}MgWO_6$
13	0	1	0	1	$Ca_{1.96}Nd_{0.02}Na_{0.02}MgWO_6$
14	0	1	0	2	$Ca_{1.94}Nd_{0.02}Na_{0.04}MgWO_6$
15	1	1	0	0	$Ca_{1.98}Nd_{0.02}Mg_{0.99}Cr_{0.01}WO_6$
16	1	1	0.5	0.5	$Ca_{1.97}Nd_{0.02}Na_{0.01}Mg_{0.985}Cr_{0.01}Li_{0.005}WO_6$
17	1	1	1	1	$Ca_{1.96}Nd_{0.02}Na_{0.02}Mg_{0.98}Cr_{0.01}Li_{0.01}WO_6$
18	1	1	1.5	1.5	$Ca_{1.95}Nd_{0.02}Na_{0.03}Mg_{0.975}Cr_{0.01}Li_{0.015}WO_6$

The samples were identified by X-ray powder diffraction (XRD) (PANalytical X'Pert Pro, Malvern Panalytical B.V., Almelo, The Netherlands) with Cu K_α radiation ($\lambda = 0.15406$ nm) operating at 40 kV and 40 mA. XRD patterns were collected from $10° \leq 2\Theta \leq 80°$.

Diffuse reflectance spectra were recorded on a FLS920 spectrometer (Edinburgh Instruments Ltd., Kirkton Campus, UK) equipped with a 450 W Xe arc lamp, a cooled (-20 °C) single-photon counting photomultiplier R2658P (Hamamatsu Photonics K.K., Hamamatsu City, Japan), and a Spectralon integration sphere. $BaSO_4$ (99.998%, Merck KGaA, Munich, Germany) was used as a reflectance standard.

The photoluminescence excitation (PLE) and emission (PL) spectra at room temperature were measured on a FLS920 spectrometer (Edinburgh Instruments Ltd., Kirkton Campus, UK) equipped with a 450 W Xe arc lamp, mirror optics for powder samples, and a cooled (-20 °C) single-photon counting photomultiplier R2658P (Hamamatsu Photonics K.K., Hamamatsu City, Japan). The decay curves were recorded on the same instrument (FLS920), and a μF900 flash lamp was used as the excitation source.

3. Results and Discussion

Ca_2MgWO_6 crystalized in a monoclinic structure with space group $P2_1/n$ and was characterized by B-Site cation ordering and $a^-a^-c^+$-type BO_6 octahedral tilting. The lattice

parameters were a = 5.4199 Å, b = 5.5479 Å, and c = 7.7147 Å [19]. Calcium atoms were co-ordinated by twelve oxygen atoms, where four oxygen atoms were significantly shortened. The average distance for the Mg–O octahedra was 2.069 Å and for the W–O octahedra was 1.922 Å, which were in good agreement with the ionic radii according to Shannon [r(Mg^{2+}) = 0.86 Å, r(W^{6+}) = 0.74 Å, r(O^{2-}) = 1.28 Å] [20].

Because of the strong ligand-field stabilization energy of Cr^{3+} ions ([Ar]$3d^3$ configuration) in sixfold coordination and the similar ionic radii between Cr^{3+} (0.755 Å) and Mg^{2+} (0.86 Å), chromium preferred to occupy octahedral magnesium sites. Another reason for occupying the magnesium sites instead of the tungsten sites was the smaller difference in ion charge. Due to the similar ionic radii, Nd^{3+} (1.410 Å) occupied Ca^{2+} (1.480 Å) lattice sites.

A charge balance was thus necessary, which was achieved by replacing Mg^{2+} with Li^+ and Ca^{2+} with Na^+ in appropriate concentration. To avoid the formation of color centers, twice the amount of charge compensation was used, which is described further on.

The XRD pattern as shown in Figure 1 proves that no changes in the crystal structure could be observed upon substituting with Cr^{3+} and Nd^{3+}. All the diffraction peaks were well indexed to those of the monoclinic Ca_2MgWO_6 phase (ICDD (International Centre for Diffraction Data): 04-012-4403).
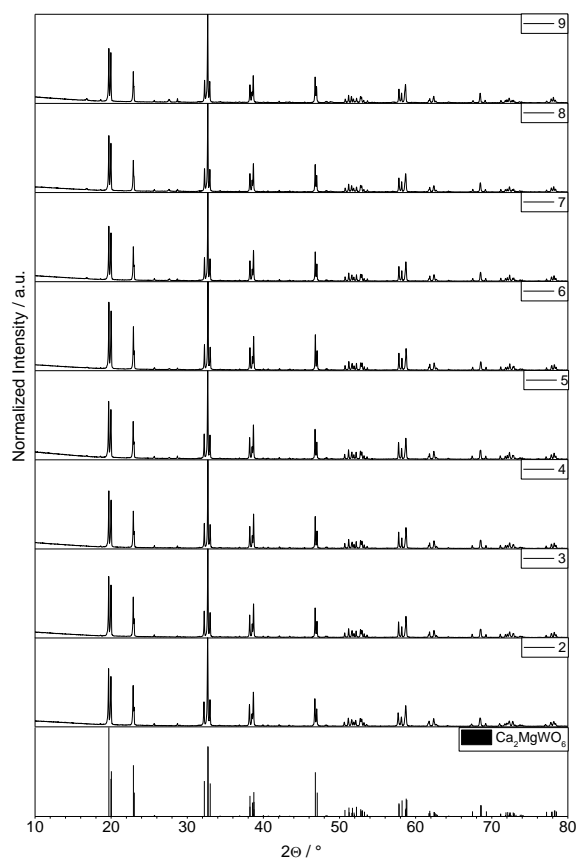

Figure 1. Room temperature X-ray diffractions (XRDs) of Cr^{3+} and Nd^{3+} co-doped Ca_2MgWO_6 samples compared to the reference from the Pearson's Crystal Database (ICDD: 04-012-4403).

Moreover, Figure 2 depicts a series of reflection spectra of Ca_2MgWO_6 in order to underline the necessity of the application of a double amount of charge compensation.

As displayed in Figure 2a Ca_2MgWO_6 was doped with Cr^{3+} and different amounts of Li^+ to reveal the effect of charge compensation. For all three samples, the three expected spin-allowed [Ar]$3d^3$–[Ar]$3d^3$ transitions of Cr^{3+} having the electron configuration [Ar]$3d^3$ were observed. These were in the UV range with its center at 345 nm ($^4A_2 \rightarrow {}^4T_1(^4P)$), in the green spectral range with its center at 475 nm ($^4A_2 \rightarrow {}^4T_1(^4F)$), and in the deep red spectral range with its center at 694 nm ($^4A_2 \rightarrow {}^4T_2(^4F)$) [17]. The sample 10 in which no

charge compensation was present showed a slightly worse reflectivity, whereas the other two samples (2 and 11) had identical reflection spectra.

Figure 2b shows the reflection spectra of the $Ca_2MgWO_6:Nd^{3+}$ samples, where the charge was balanced with different amounts of Na^+. Again, only a slight improvement of the reflectivity could be observed. For all three samples (12–14), the typical 4f–4f-transitions of Nd^{3+} were observed. These were located at 530 nm ($^4I_{9/2} \rightarrow {}^4G_{7/2}$), 590 nm ($^4I_{9/2} \rightarrow {}^4G_{5/2}$), 685 nm ($^4I_{9/2} \rightarrow {}^4F_{9/2}$), and 750 nm ($^4I_{9/2} \rightarrow {}^4F_{7/2}$).

Figure 2c shows the reflection spectra of Ca_2MgWO_6 samples co-doped with Cr^{3+} and Nd^{3+}, where the charge was balanced with different amounts of Li^+/Na^+ (samples 4 and 15–18). In contrast to $Ca_2MgWO_6:Cr^{3+}$ and $Ca_2MgWO_6:Nd^{3+}$, another very broad absorption band was recorded, which only occurred if Cr^{3+} and Nd^{3+} were present at the same time. Therefore, we assumed the presence of a charge transfer transition between Cr^{3+} and Nd^{3+}. This charge transfer was significantly suppressed by the addition of Li^+/Na^+ due to the better ion distribution, and thus this additional absorption band disappeared gradually until the amount of charge compensation was doubled. Then, only the typical spin-allowed transitions of Cr^{3+} and the spin-forbidden transitions of Nd^{3+} were visible.

Therefore, the reflection spectra of samples shown in Figure 2d ($Ca_2MgWO_6:1\%Cr,y\%Nd$) were synthesized with just this required amount of Li^+/Na^+ (Samples 2–9). Additionally, the undoped compound (Sample 1) was plotted here, which was used to determine the band gap of Ca_2MgWO_6, which was derived to be 4.0 eV. As described above, one could observe the transitions of Cr^{3+} as well as the transitions of Nd^{3+}. As the proportion of Nd^{3+} increased, the absorption lines of Nd^{3+} gained more intensity.
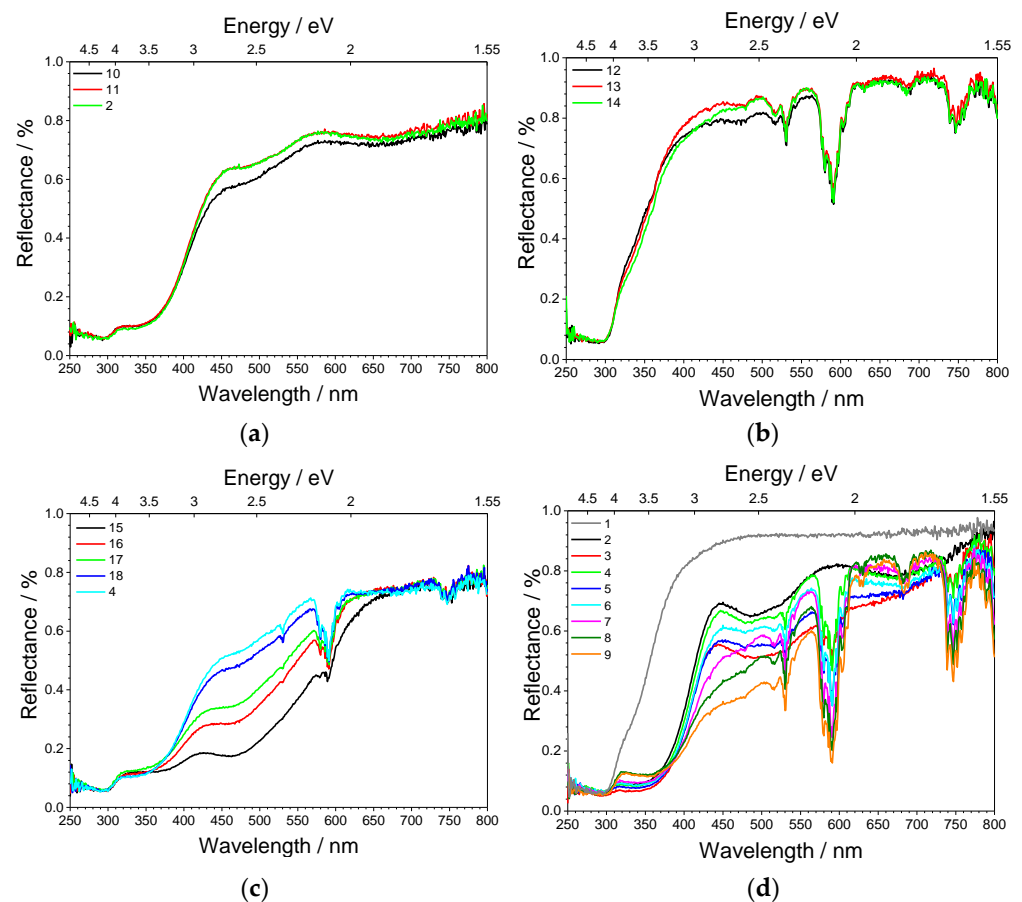

Figure 2. Diffuse reflection spectra of Ca_2MgWO_6 with (**a**) 1% Cr^{3+} and different amounts of Li^+; (**b**) 1% Nd^{3+} and different amounts of Na^+; (**c**) 1% Cr^{3+}, 1% Nd^{3+} and different amounts of Li^+ and Na^+; and (**d**) 1% Cr^{3+}, (0–8)% Nd^{3+} and double amount of Li^+ and Na^+.

Figure 3 shows the excitation spectra of Ca_2MgWO_6 doped with 1% Cr^{3+} and a variable content of Nd^{3+} between 0 and 8 atom-%. The emission monochromator in Figure 3a was fixed to the emission of the Cr^{3+} emission band at 825 nm, while in Figure 3b, it was set to the line emission of Nd^{3+} located at 879 nm.
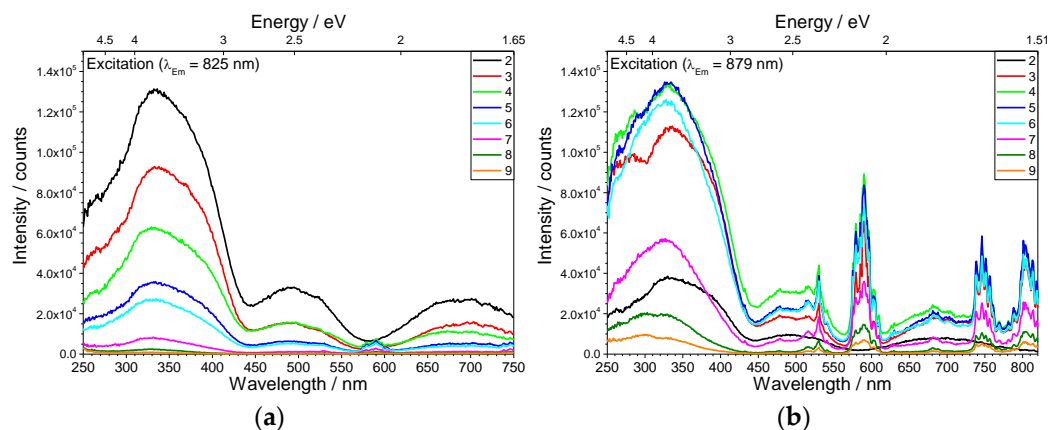

Figure 3. Excitation spectra of Ca_2MgWO_6 doped with 1% Cr^{3+} and (0–8)% Nd^{3+} and double amount of Li^+ and Na^+; (**a**) emission monochromator fixed at emission line of Cr^{3+} (825 nm), (**b**) emission monochromator fixed at emission line of Nd^{3+} (879 nm).

In the excitation spectrum monitoring the Cr^{3+} emission, all three expected 3d–3d excitation bands were seen in the UV (maximum at 330 nm), the green (maximum at 490 nm), and the deep red (maximum at 687 nm) spectral range. They could be clearly assigned to the spin-allowed crystal-field transitions $^4A_2 \rightarrow {}^4T_1(^4P)$, $^4A_2 \rightarrow {}^4T_1(^4F)$, and $^4A_2 \rightarrow {}^4T_2(^4F)$ of Cr^{3+}. However, the high intensity of the former transition in this compound was not typical, which showed a comparison to other Cr^{3+} doped compounds. Mostly, the two transitions in the visible spectral region exhibited much higher intensity [21–24]. The decrease in excitation intensity occurred with increasing content of Nd^{3+}, as expected for efficient energy transfer from Cr^{3+} to Nd^{3+}. The excitation lines visible at about 580 nm, which were caused by the presence of Nd^{3+}, point to the presence of back transfer from Nd^{3+} to Cr^{3+}, because there were no Nd^{3+} emission lines in the emission range set here.

The excitation spectrum of Nd^{3+} emission also showed the three typical broad excitation bands of Cr^{3+} in the UV, the green, and the deep red spectral range, which also confirmed efficient energy transfer from Cr^{3+} to Nd^{3+}. In addition, excitation lines were found at 530 nm, 590 nm, 750 nm, and 800 nm, which could be assigned to the intraconfigurational 4f–4f transitions $^4I_{9/2} \rightarrow {}^4G_{7/2}$, $^4I_{9/2} \rightarrow {}^4G_{5/2}$, $^4I_{9/2} \rightarrow {}^4F_{7/2}$, and $^4I_{9/2} \rightarrow {}^4F_{5/2}$ of Nd^{3+}.

Figure 4 depicts the emission spectra of the compounds Ca_2MgWO_6:1%Cr,*y*%Nd, whereby y was between 0 and 8. In the absence of Nd^{3+} (sample 2), solely the broadband emission of Cr^{3+} was visible ($^4T_2 \rightarrow {}^4A_2$), which was located between 700 and 1000 nm and culminated at 825 nm. After adding the Nd^{3+}, the emission intensity of the Cr^{3+} transition decreased, and new emission lines could be measured in the spectral range between 870 and 930 nm. Up to a Nd content of 1.5% (Sample 5), the Nd^{3+} emission intensity increased due to the gradually promoted energy transfer, while at even higher concentrations, it declined again due to concentration quenching.
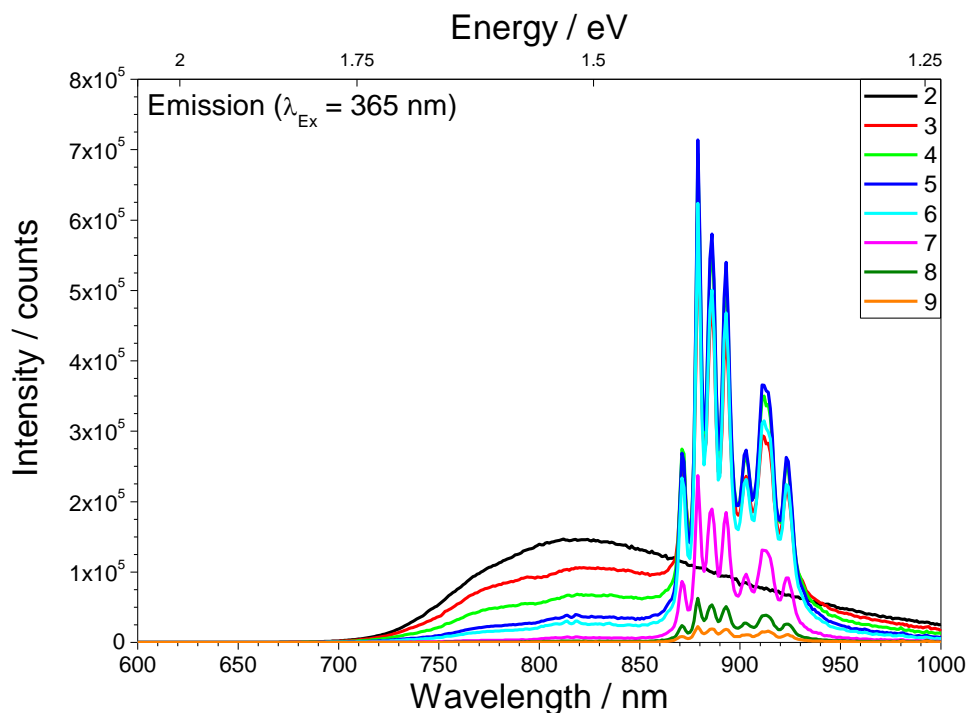
Figure 4. Emission spectra of Ca_2MgWO_6 doped with 1% Cr^{3+} and (0–8)% Nd^{3+} and double amount of Li^+ and $Na^{+.}$

Figure 5 shows the decay curves of the compounds Ca_2MgWO_6:1%Cr, y%Nd, with excitation at λ_{Ex} = 365 nm in each case.

In Figure 5a, the Cr^{3+} emission subsequent to UV-A excitation was observed at 825 nm. If only Cr^{3+} ions were present (Sample 2), a monoexponential decay curve was observed, which could be fitted with a decay time of τ = 28 μs. This fit very well with a spin-allowed transition originating from the $^4T_2$ state. Upon co-doping with Nd^{3+} ions, biexponential decay curves were just obtained, with the first component decaying faster and the second component decaying much more slowly than observed for the sample without Nd^{3+}. From this, it can be concluded that the energy was firstly transferred to the Nd^{3+} ions, and, secondly, back transfer to the Cr^{3+} ions occurred. The more Nd^{3+} ions were present in the compound (Samples 8 and 9), the more the observed decay curve could be approached by a monoexponential function. This points to the conclusion that the back transfer was no longer the rate-determining step.

In Figure 5b, the emission was observed at 879 nm. If solely Cr^{3+} ions were present Sample 2), a monoexponential decay behavior was present, which corresponded to the previously described decay behavior of Cr^{3+}. By co-doping with Nd^{3+} ions, biexponential decay curves with significantly delayed decay behavior were initially obtained. With a further increase of the Nd^{3+} concentration (Sample 6), there was a monoexponential decay curve yielding a decay time of 120 μs. A further increase led again to a biexponential decay curve but with a shorter decay time compared to the previous samples.
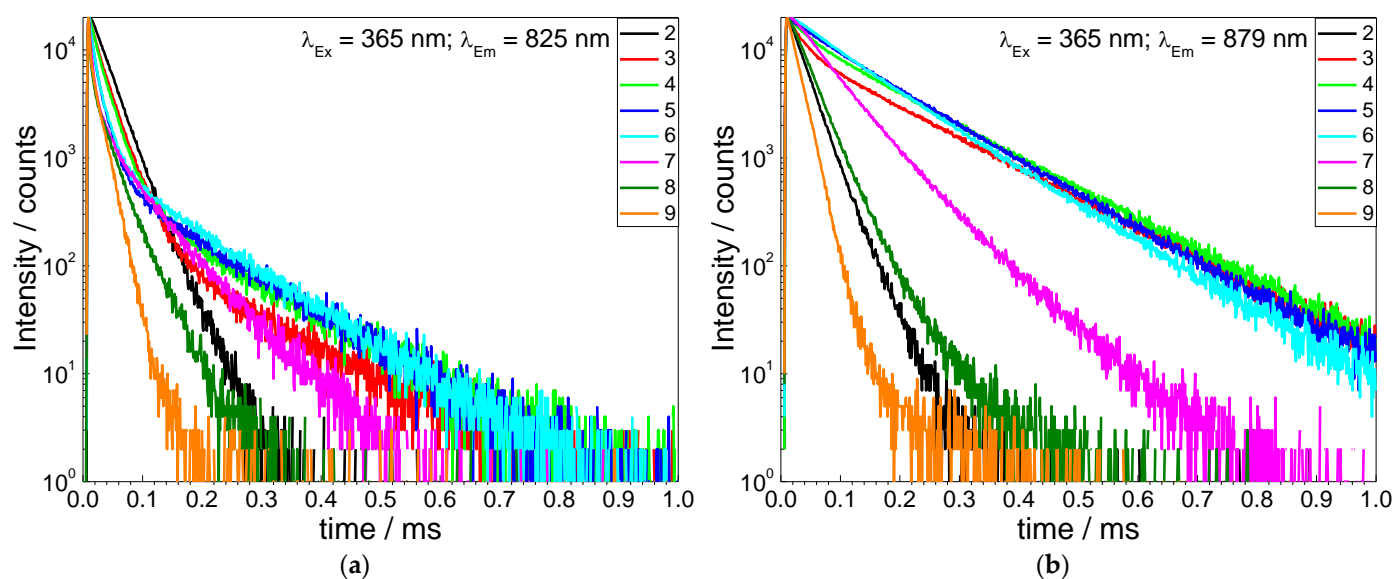
Figure 5. Decay curves of Ca_2MgWO_6 doped with 1% Cr^{3+} and (0–8)% Nd^{3+} and double amount of Li^+ and Na^+; (**a**) emission monochromator fixed at emission line of Cr^{3+} (825 nm), (**b**) emission monochromator fixed at emission line of Nd^{3+} (879 nm).

4. Conclusions

In summary, a set of single phase samples of Ca_2MgWO_6:Cr^{3+},Nd^{3+} were prepared by a conventional solid state reaction due to sintering at 1300 °C. Additionally, the synthesis procedure of this material was optimized by adding the double molar amount of Li^+ and Na^+ for charge compensation. The presence of highly pure samples and the lack of the formation of color centers were confirmed by reflection spectra.

Photoluminescence properties were also studied in detail. The excitation spectra of the Cr^{3+} activator extended from 250 to 750 nm, while the emission spectra of the Cr^{3+} spread out from 700 to 1000 nm. Efficient energy transfer occurred from Cr^{3+} to Nd^{3+}, which was proven by the decline of luminescence intensity and the decay time of Cr^{3+} by ascending the concentration of the co-dopant Nd^{3+}. Since the activator Cr^{3+} exhibited broadband absorption between 250 and 750 nm, especially between 250 and 430 nm, and Nd^{3+} emit in the NIR range, the Ca_2MgWO_6:Cr^{3+},Nd^{3+} phosphors are promising materials to be employed as luminescent converters in ultraviolet (Al,Ga)N or near UV (In,Ga)N emitting LEDs.

Author Contributions: Writing—original draft, V.A.; Writing—review & editing, T.J. All authors have read and agreed to the published version of the manuscript.

Institutional Review Board Statement: Not applicable.

Informed Consent Statement: Not applicable.

Data Availability Statement: Not applicable.

Conflicts of Interest: The authors declare no conflict of interest.

References

1. Zabiliūtė-Karaliūnė, A.; Dapkus, H.; Petrauskas, R.P.; Butkutė, S.; Žukauskas, A.; Kareiva, A. Cr^{3+} doped yttrium gallium garnet for phosphor-conversion light emitting diodes. *Lith. J. Phys.* **2015**, *55*, 200–207. [CrossRef]
2. Martin, P.A. Near-infrared diode laser spectroscopy in chemical process and environmental air monitoring. *Chem. Soc. Rev.* **2002**, *31*, 201–210. [CrossRef] [PubMed]

3. Godavarty, A.; Thompson, A.B.; Roy, R.; Gurfinkel, M.; Eppstein, M.J.; Zhang, C.; Sevick-Muraca, E.M. Diagnostic imaging of breast cancer using fluorescence-enhanced optical tomography: Phantom studies. *J. Biomed. Opt.* **2004**, *9*, 488–496. [CrossRef]

4. Blanco, M.; Villarroya, I. NIR spectroscopy: A rapid-response analytical tool. *Trends Anal. Chem.* **2002**, *21*, 240–250. [CrossRef]

5. Min, P.K.; Goo, B.L. 830 nm light-emitting diode low level light therapy (LED-LLLT) enhances wound healing: A preliminary study. *Laser Ther.* **2013**, *22*, 43–49. [CrossRef] [PubMed]

6. Usamentiaga, R.; Venegas, P.; Guerediaga, J.; Vega, L.; Molleda, J.; Bulnes, F.G. Infrared thermography for temperature measurement and non-destructive testing. *Sensors* **2014**, *14*, 12305–12348. [CrossRef]

7. Han, C.B.; He, C.; Li, X.J. Near-infrared light emission from a GaN/Si nanoheterostructure array. *Adv. Mater.* **2011**, *23*, 4811–4814. [CrossRef]

8. Xia, Q.; Batentschuk, M.; Osvet, A.; Richter, P.; Häder, D.P.; Schneider, J.; Brabec, C.J.; Wondraczek, L.; Winnacker, A. Enhanced photosynthetic activity in Spinacia oleracea by spectral modification with a photoluminescent light converting material. *Opt. Express* **2013**, *21* (Suppl. S6), A909–A916. [CrossRef]

9. Zhu, J.; Xia, Z.; Liu, Q. Synthesis and energy transfer studies of $LaMgAl_{11}O_{19}:Cr^{3+},Nd^{3+}$ phosphors. *Mater. Res. Bull.* **2016**, *74*, 9–14. [CrossRef]

10. Patwe, S.J.; Achary, S.N.; Mathews, M.D.; Tyagi, A.K. Crystal structure and thermal expansion behavior of Ca_2MgWO_6. *Mater. Chem. Phys.* **2006**, *98*, 486–493. [CrossRef]

11. Lei, F.; Yan, B. Synthesis and photoluminescence of perovskite-type $Ca_2MgWO_6:Eu^{3+}$ micrometer phosphor. *Optoelectron. Adv. Mater. Rapid Commun.* **2008**, *10*, 158–163.

12. Cao, R.; Quan, G.; Shi, Z.; Luo, Z.; Hu, Q.; Guo, S. A double perovskite $Ca_2MgWO_6:Bi^{3+}$ yellow-emitting phosphor: Synthesis and luminescence properties. *J. Lumin.* **2017**, *181*, 332–336. [CrossRef]

13. Cao, R.; Xu, H.; Luo, W.; Luo, Z.; Guo, S.; Xiao, F.; Ao, H. Synthesis, energy transfer and luminescence properties of $Ca_2MgWO_6:Sm^{3+}$, Bi^{3+} phosphor. *Mater. Res. Bull.* **2016**, *81*, 27–32. [CrossRef]

14. Cui, M.; Wang, J.; Li, J.; Huang, S.; Shang, M. An abnormal yellow emission and temperature-sensitive properties for perovskite-type Ca_2MgWO_6 phosphor via cation substitution and energy transfer. *J. Lumin.* **2019**, *214*, 116588. [CrossRef]

15. Jiang, Y.; Tong, Y.; Chen, S.; Zhang, W.; Hu, F.; Wei, R.; Guo, H. A three-mode self-referenced optical thermometry based on up-conversion luminescence of $Ca_2MgWO_6:Er^{3+},Yb^{3+}$ phosphors. *Chem. Eng. J.* **2021**, *421*, 127470. [CrossRef]

16. Chen, X.; Zhao, T.; Qin, L. The red-emitting phosphors of Mn^{4+}-activated A_2MgWO_6 (A = Ba, Sr, Ca) for light emitting diodes. *Ceram. Int.* **2021**, *47*, 6010–6022. [CrossRef]

17. Xu, D.; Wu, X.; Zhang, Q.; Li, W.; Wang, T.; Cao, L.; Meng, J. Fluorescence property of novel near-infrared phosphor $Ca_2MgWO_6:Cr^{3+}$. *J. Alloy. Compd.* **2018**, *731*, 156–161. [CrossRef]

18. Xu, D.; Zhang, Q.; Wu, X.; Li, W.; Meng, J. Synthesis, luminescence properties and energy transfer of $Ca_2MgWO_6:Cr^{3+},Yb^{3+}$ phosphors. *Mater. Res. Bull.* **2019**, *110*, 135–140. [CrossRef]

19. Yang, J.H.; Choo, W.K.; Lee, C.H. Ca_2MgWO_6 from neutron and X-ray powder data. *Acta. Crystallogr. C* **2003**, *59*, i86–i88. [CrossRef]

20. Shannon, R.D.; Prewitt, C.T. Effective ionic radii in oxides and fluorides. *Acta. Crystallogr. B Struct. Sci.* **1969**, *25*, 925–946. [CrossRef]

21. Malysa, B.; Meijerink, A.; Jüstel, T. Temperature dependent luminescence Cr^{3+}-doped $GdAl_3(BO_3)_4$ and $YAl_3(BO_3)_4$. *J. Lumin.* **2016**, *171*, 246–253. [CrossRef]

22. Malysa, B.; Meijerink, A.; Wu, W.; Jüstel, T. On the influence of calcium substitution to the optical properties of Cr^{3+} doped $SrSc_2O_4$. *J. Lumin.* **2017**, *190*, 234–241. [CrossRef]

23. Malysa, B.; Meijerink, A.; Jüstel, T. Temperature dependent photoluminescence of Cr^{3+} doped $Sr_8MgLa(PO_4)_7$. *Opt. Mater.* **2018**, *85*, 341–348. [CrossRef]

24. Anselm, V.; Jüstel, T. On the photoluminescence and energy transfer of $SrGa_{12}O_{19}:Cr^{3+},Nd^{3+}$ microscale NIR phosphors. *J. Mater. Res. Technol.* **2021**, *11*, 785–791. [CrossRef]